

Understanding and Hindering the Electron Leakage in Green InP Quantum-Dot Light-Emitting Diodes

Tianqi Zhang, Fangqing Zhao, Pai Liu, Yangzhi Tan, Xiangtian Xiao, Zhaojin Wang, Weigao Wang, Dan Wu, Xiao Wei Sun, Jianhua Hao, Guichuan Xing,* and Kai Wang*

Indium phosphide (InP) quantum-dot light-emitting diodes (QLEDs) are considered as one of the most promising candidates for emerging displays owing to their good luminous performance and environmentally friendly properties. The operation of green InP QLEDs relies on the radiative recombination of electrically generated excitons, as in most QLEDs; however, the electrons injected into green InP QLEDs can easily pass through the quantum-dot (QD) layer, resulting in a carrier imbalance and low external quantum efficiency (EQE). Herein, the mechanism of electron leakage in green InP QLEDs is revealed. Based on comparative experiments and simulations of the carrier concentration distribution, the path of electron leakage is determined and it is found that the root cause is the large Fermi energy difference between green InP QDs and indium tin oxide (ITO). To solve this problem, an ultrathin LiF layer is applied to modify the work function of the ITO, which simultaneously hinders electron leakage and enhances hole injection. Benefiting from a more balanced carrier injection, the maximum EQE of green InP QLEDs improves from 4.70% to 9.14%. In these findings, a universal mechanism is provided for hindering electron leakage in green InP QLEDs, indicating the feasibility of developing highly efficient green InP QLEDs.

solution processability, InP QDs are more environmentally friendly than traditional Cd-based QDs.^[10–12] Hence, electroluminescent devices such as InP QLEDs are considered some of the most promising candidates for display applications. In recent years, the photoluminescence quantum yield (PLQY) of green InP QDs (>95%) has matched that of Cd-based QDs^[10] and many common optimizations of device structures used in Cd-based QLEDs have been applied to green InP QLEDs.^[13–15] However, although a maximum external quantum efficiency (EQE) of 16.3% has recently been achieved,^[16] the lack of an in-depth understanding of carrier imbalance in green InP QLEDs still limits their performance.


In previous studies on green InP QLEDs, parasitic emissions caused by carrier imbalances have been reported.^[17–22] Yang et al. proposed the poor electron confinement effect of InP/ZnS QDs as a reasonable cause for the emission from hole-transport layers (HTLs).^[17,18]

Considering that the ZnS shell is not uniform because of its large lattice mismatch with the InP core, Lim et al. replaced InP/ZnS QDs with InP/ZnSeS QDs and optimized the distribution of the chemical composition of the shell.^[19] Benefiting from the larger QDs with thicker ZnSeS alloy shells, a balance between the alleviation of the lattice strain was achieved. Hence, better confinement of electrons suppressed the parasitic emission. With

1. Introduction

Indium phosphide (InP) quantum dots (QDs) are promising cadmium-free nanocrystalline materials as the emissive layer for high-performance QD light-emitting diodes (QLEDs).^[1–9] In addition to their extraordinary merits, including tunable spectrum, high color saturation, low energy consumption, and simple

T. Zhang, F. Zhao, P. Liu, Y. Tan, X. Xiao, Z. Wang, W. Wang, X. W. Sun, K. Wang
Institute of Nanoscience and Applications, and Department of Electrical and Electronic Engineering
Key Laboratory of Energy Conversion and Storage Technologies
Ministry of Education
Southern University of Science and Technology
Shenzhen 518055, China
E-mail: wangk@sustech.edu.cn

 The ORCID identification number(s) for the author(s) of this article can be found under <https://doi.org/10.1002/adpr.202300146>.

© 2023 The Authors. Advanced Photonics Research published by Wiley-VCH GmbH. This is an open access article under the terms of the Creative Commons Attribution License, which permits use, distribution and reproduction in any medium, provided the original work is properly cited.

DOI: 10.1002/adpr.202300146

T. Zhang, G. Xing
Institute of Applied Physics and Materials Engineering
University of Macau
Macau 999078, China
E-mail: gcxing@um.edu.mo

F. Zhao, J. Hao
Department of Applied Physics
The Hong Kong Polytechnic University
Hong Kong 999077, China

D. Wu
College of New Materials and New Energies
Shenzhen Technology University
Shenzhen 518118, China

the optimization of InP QDs materials and the selection of non-luminous HTLs, the phenomenon of parasitic emissions is no longer common in recent reports. However, the nonradiative recombination of carriers in HTLs still affects the efficiency of green InP QLEDs. In 2020, Deng et al. suggested that, for the charge leakage in QLEDs, electrons leaked from charged QDs to HTLs in the form $QD^- + HTL \rightarrow QD + HTL^-$.^[23] This mechanism is applicable to most CdSe-based QLEDs. However, the significant electron leakage phenomenon in green InP QLEDs is difficult to explain. Therefore, the special electron leakage mechanism in green InP QLEDs must be urgently explored to understand their carrier imbalances.

In this article, we address the fundamental question of how the electrons leak from green InP/ZnS QDs and propose an effective solution. Using comparative experiments, we observed that electrons diffuse between the green InP/ZnS QDs layer and the other functional layers. Further simulation of the carrier concentration distribution supported that some of the electrons in the green InP QDs leak toward the side of the indium tin oxide (ITO) owing to their Fermi energy difference. Such electron leakage reduces radiation recombination in the QDs layer, resulting in a low EQE for green InP QLEDs. To hinder electron leakage, we modified the work function (WF) of the ITO using a LiF layer to reduce the Fermi energy difference between the green InP QDs and ITO. Meanwhile, the tunneling effect caused by the ultrathin LiF layer further enhanced hole injection in the device. Compared with the contrast device, the maximum luminance of green InP QLEDs was enhanced from 22 149 to 32 380 cd m^{-2} , and the maximum EQE improved from 4.70%@5.92 mA cm^{-2} (No LiF) to 9.14%@12.83 mA cm^{-2} (1.0 nm LiF), an enhancement of approximately two times. This article revealed the electron leakage mechanism in green InP QLEDs and proposed an effective solution. A unique mechanism is described to interpret the electron leakage driven by the Fermi energy difference between the QDs and the ITO anode.

2. Simulation and Experiment

2.1. Simulation

The carrier concentration distributions were simulated using COMSOL Multiphysics software. The carrier distribution models used in the simulations were based on Poisson's equation and the continuity equation, whereas the carrier concentration change followed the drift–diffusion equation. The energy band information used in the simulations was obtained from reference^[24] and the Fermi-level data were obtained from ultraviolet photoelectron spectroscopy (UPS) spectra.

Electrical simulations of the recombination rate were performed using the software Setfos 4.6, and constant or field-dependent electron and hole mobilities according to the Poole–Frenkel model were used in the simulations. The selected highest occupied molecular orbital (HOMO)/lowest unoccupied molecular orbital (LUMO) values are shown in Figure 2a. The energy level data and carrier mobilities information used in simulations are shown in Table S1, Supporting Information. Boundary conditions for the charge carrier densities at the electrodes were set to satisfy the Fermi-level alignment at thermal

equilibrium. Exciton generation was permitted only in the emission layer and followed the standard Langevin recombination.

2.2. Materials

Poly (3,4-ethylenedioxythiophene):poly(styrenesulfonate) (PEDOT:PSS, Clevious P VP Al 4083) was purchased from Xi'an p-OLED Ltd. and used directly without further dilution. Poly(9-vinylcarbazole) (PVK) was purchased from Lumtec Ltd. and dissolved in chlorobenzene at 8 mg mL^{-1} . Green InP/ZnS QDs were purchased from Fullnano Ltd. and dissolved in octane at 10 mg mL^{-1} . The diameter of green InP/ZnS QDs was 5.0 ± 0.2 nm and the ligands were trioctylphosphine (TOP) and oleic acid (OA). ZnMgO nanoparticles were purchased from Mesolight Ltd., and suspended in ethanol at 20 mg mL^{-1} . LiF was purchased from Lumtec Ltd.

2.3. Device Fabrication

The QLED devices were fabricated with the structure of ITO/LiF (0, 0.5, 0.75, 1.0, 1.25, 1.5, 1.75, and 2.0 nm)/PEDOT:PSS (25 nm)/PVK (30 nm)/QDs (25 nm)/ZnMgO (30 nm)/Al (100 nm). The half-devices in the photoluminescence (PL) comparative experiments were fabricated using the structures shown in Figure 1a and their thicknesses were the same as those of the actual QLED device. Hole-only devices (HODs) were fabricated with the following structure: ITO/LiF (0, 0.5, 1.0, 1.5, and 2.0 nm)/PEDOT:PSS (25 nm)/PVK (30 nm)/green InP/ZnS QDs (25 nm)/tris (4-carbazoyl-9-ylphenyl)amine (TCTA) (10 nm)/N,N'-Di(1-naphthyl)-N,N'-diphenyl-(1,1'-biphenyl)-4,4'-diamine (NPB) (10 nm)/1,4,5,8,9,11-hexaazatriphenylenehexacarbonitrile (HAT-CN) (15 nm)/Al (100 nm). The patterned ITO electrodes were cleaned and treated with plasma before use. All functional layers, except LiF, were deposited via spin-coating at 3000 rpm for 45 s with the assistance of thermal annealing. LiF and Al electrodes were deposited using thermal evaporation at average rates of 0.1 and 0.2 nm s^{-1} , respectively, under a vacuum of 5×10^{-4} Pa.

2.4. Characterization

The energy level information used in the simulations was measured in the film form using UPS (PHI 5000 Versaprobe III system), and a -3 V bias voltage was applied. The luminance of the device was 2×2 mm. The PLQY and PL spectra were measured at an excitation wavelength of 365 nm using an absolute PLQY spectrometer (Hamamatsu Quantaurus QY C11347-12). The devices were assumed to be Lambert illuminated, and the current density–voltage–luminance (J – V – L) curves were measured using a Keithley 2614 B source and a PIN-25D silicon photodiode. All the measurements were performed at room temperature (25 °C).

3. Results and Discussion

Electron diffusion from the green InP/ZnS QDs was observed during PL characterization. In this study, four layers of green InP/ZnS QDs films were coated onto 1) glass/ITO, 2) glass/ITO/polyvinylpyrrolidone (PVP), 3) ITO/glass, and 4) ITO/glass/PVP (Figure 1a).

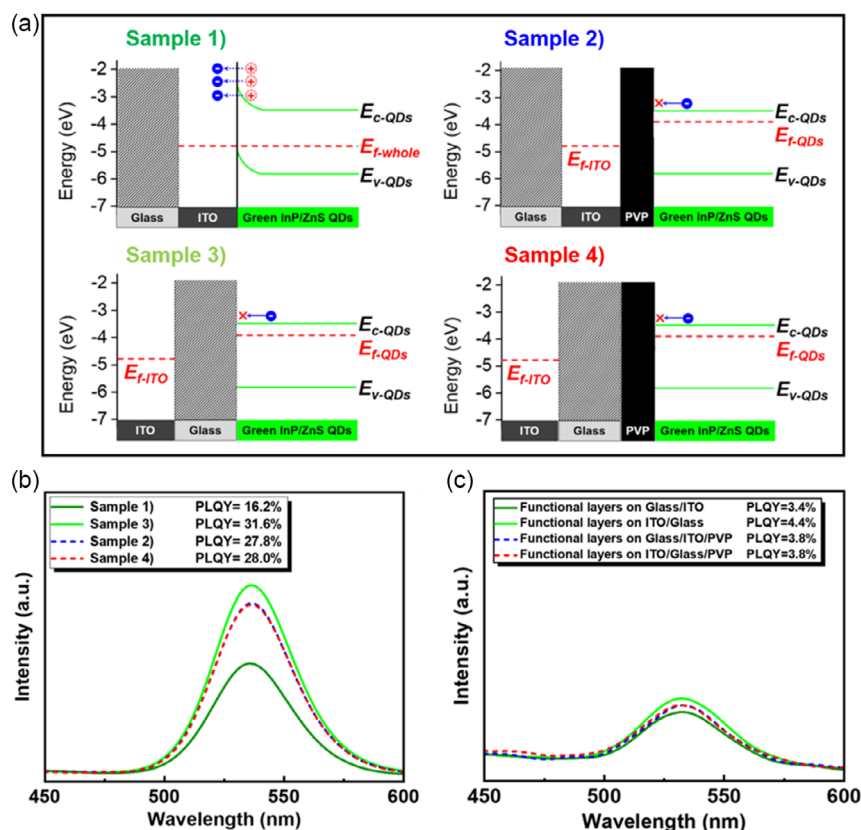


Figure 1. a) Schematics of green InP/ZnS quantum dots (QDs) films on the four types of substrates as glass/ITO, glass/ITO/PVP, ITO/glass, and ITO/glass/PVP. b) Photoluminescence (PL) spectra of the samples. c) PL spectra of the functional layers Poly(3,4-ethylenedioxythiophene):poly(styrenesulfonate) (PEDOT:PSS)/poly(9-vinylcarbazole) (PVK)/green InP/ZnS QDs/ZnMgO on the four types of substrates.

Compared with the control sample 1, sample 3 reversed the front and back surfaces of the ITO glass. The glass substrate cut off the Schottky contact between the QDs and ITO while ensuring similar light absorption. Moreover, the validation samples 2 and 4 introduced insulating PVP layers between their substrates and QDs layers to arrest electron diffusion. As shown in Figure 1b, the PLQY of sample 1 on the ITO side was 16.2%, which was 48.7% lower than that of sample 3 on the glass side (PLQY = 31.6%). Samples 2 and 4 with a PVP interlayer achieved a PLQY of $\approx 28.0\%$. The insulating glass and PVP between the green InP/ZnS QDs and ITO effectively prevented a reduction in the PL intensity of the samples. This implied that electron diffusion occurs between the QDs and ITO, which is considered to be caused by Schottky contact. To verify this hypothesis, absorption spectra and UPS measurements were performed to identify the Fermi level of the green InP QDs. The results are shown in Figure S1, Supporting Information. The Fermi level of green InP/ZnS QDs was obtained as -3.72 eV. The conduction band minimum (CBM) and valence band maximum were -3.53 and -5.99 eV, respectively. The shallow energy band of green InP QDs has been reported in many papers.^[18–20,25–27] The Fermi level of the green InP QDs was closer to that of the CBMs because of the characteristics of n-type materials. This was shallower than the Fermi level of ITO (-4.8 eV); thus, the electrons diffused from the green InP QDs to the ITO electrode. To further study

whether this electron diffusion occurs in green InP QLEDs, we coated all the functional layers, such as PEDOT:PSS/PVK/green (InP/ZnS) QDs/ZnMgO, on the aforementioned four substrates according to the actual QLED device structure. The PLQY of the sample fabricated on glass/ITO was 3.4%, which was 22.7% lower than that of the sample fabricated on ITO/glass (4.4%) (Figure 1c). Although Schottky contact frequently occurs at the material interface, these results imply similar electron diffusion in actual devices. Therefore, a deeper understanding of this electron diffusion phenomenon is urgent, which would be useful for further enhancing the performance of green InP QLEDs.

To further study the diffusion of electrons, we simulated the electron concentrations of the functional layers in the green InP QLED devices. The energy band and Fermi level information used in the simulation are shown in Figure 2a. The separated functional layers were simulated as references for the original electron concentrations (Figure 2b). Subsequently, the function layers were arranged and contacted completely according to the actual green InP QLED device to simulate scenarios with and without a bias voltage. In the simulation, we focused on the relative distribution of the electron concentration in the function layers and set 5 V as the bias voltage because QLEDs can operate stably at this voltage. Because metal characteristics with high electron concentrations are not applicable to the semiconductor model, Al and ITO electrodes were set to metal boundary

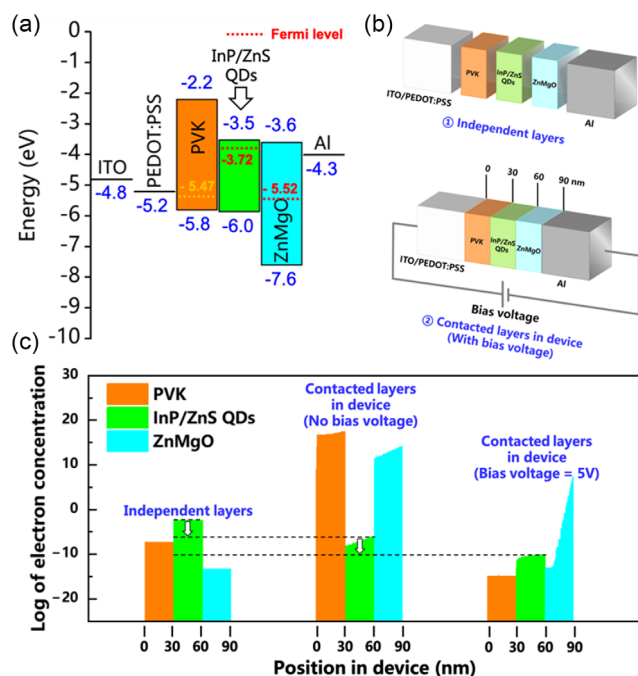


Figure 2. a) Energy band and Fermi level of each material in the quantum-dot light-emitting diode (QLED). b) Schematic of QLED models in carrier concentration simulations. c) Simulation of the electron concentration in independent layers and the contacted layers in the green InP QLEDs with/without a 5 V bias voltage.

conditions with the corresponding WF in the simulation, instead of as separate layers. The PEDOT:PSS layer is generally used together with the ITO anode because of its high conductivity.^[28,29] This can be observed in the results in Figure 2c: the electron concentrations in the PVK and ZnMgO layers were dozens of orders of magnitude higher than their original levels in the independent layers. However, the green InP/ZnS QDs layer had an electron concentration five orders of magnitude lower than that of the green CdSe/ZnS QDs in the CdSe QLEDs (Figure S2, Supporting Information). This indicated that no net electron diffusion occurred into the green InP/ZnS QDs layer, but electrons leaked out. When the bias voltage was increased to 5 V, a high electron concentration still existed in ZnMgO on the side in contact with the Al cathode. However, the electron concentration of ZnMgO near the green InP/ZnS QDs side decreased to a low level, indicating that the electrons injected into ZnMgO partially migrated to the QDs layer. Additionally, the electron concentration of the green InP/ZnS QDs further decreased, indicating that the injected electrons were not confined to this layer. Because of the closed circuit, electrons in PVK were rapidly transferred to the ITO anode; thus, a low electron concentration was also present in the PVK layer. Interestingly, in the green CdSe QLEDs, the electron concentration in the QDs layer remained higher than the original level (Figure S2, Supporting Information). Such an electron leakage phenomenon might be an important reason the performance of green InP QLEDs lagged that of green CdSe QLEDs.

Based on the experimental phenomena and simulation results, a new understanding of the electron leakage mechanism

in green InP QLEDs is proposed in this article (Figure 3). The gaps in the schematic indicate that the layers were independent. When the ITO/PEDOT:PSS and Al contact PVK and ZnMgO, respectively, as Schottky contacts (Figure 3b), electrons diffuse into the material at deeper Fermi levels, as indicated by the blue dashed line. Subsequently, the electron concentration in the transport layer increases significantly, and the Fermi levels of the HTL and electron transport layer (ETL) shift to E_{f-p} and E_{f-n} . Because the green InP/ZnS QDs layer has a shallow Fermi level, both E_{f-p} and E_{f-n} are deeper than $E_{f-G-InP}$ in the complete QLED device (Figure 3b). Therefore, electrons in the green InP QDs leak to both sides: the ZnMgO/Al and the ITO electrode sides. Similar to the electron diffusion in heterojunctions, the leaked electrons bend the energy bands (Figure 3c). Under the influence of the built-in electric field at the interfaces, dynamic equilibrium is maintained, and further leakage of electrons on the two sides is inhibited. For devices operating under a bias voltage, the built-in electric field is offset by an inverse external electric field.^[30] Subsequently, the bent energy band flattens again and the electrons continue to leak to the HTL side (Figure 3d). Although electrons tend to diffuse to the ETL side, they are restrained under bias because of the single direction of electron transport. Notably, the direction of the electron migration is also from the Al cathode to the ITO anode. The dual effects of diffusion and migration lead to excess electrons in the HTL; thus, the imbalance of carriers is severer, resulting in nonradiative recombination at the HTL and a lower EQE of the QLEDs, as mentioned previously. In contrast to the green InP QLEDs, E_{f-p} is still higher than E_{f-CdSe} in the green CdSe QLEDs; thus, electrons tend to accumulate in the green CdSe/ZnS QDs with a deep Fermi level (Figure S3, Supporting Information). Less nonradiative recombination would occur at the HTL; thus, more holes can be transferred to the QDs layer, ensuring a high EQE of green CdSe QLEDs.

To prevent electron leakage caused by the difference in the Fermi energy, an ultrathin LiF layer is used to reduce the WF of the ITO electrode. In common OLED/QLED research, LiF is used as a hole barrier layer or to modify the Al cathode to affect electron injection.^[7,31,32] In this study, the WF_{ITO} exhibited a significant change from 4.82 to 4.41 eV when the thickness of LiF was adjusted, and the UPS results are shown in Figure S4, Supporting Information. As previously analyzed, the reduction in WF_{ITO} increased E_{f-p} (Figure 4a). Therefore, the difference between E_{f-p} and $E_{f-G-InP}$ decreased. The electron leakage from the green InP/ZnS QDs was significantly inhibited, regardless of the bias voltage. As a result, this modification changed the electron concentration in the green InP QLEDs (Figure 4b). The electron concentration in the green InP/ZnS QDs layer significantly increased after the ITO was modified using LiF. In the case without a bias voltage, the electron concentration in the green InP/ZnS QDs layer was higher than the original level in the independent layer (gray dashed line) when WF_{ITO} was 4.41 eV. This confirmed that electrons accumulated in the QDs layer, similar to the phenomenon observed in the green CdSe QLEDs. The radiation recombination rate was simulated to further verify the confinement of electron leakage. Benefitting from the hindered electron leakage, holes underwent radiative recombination with electrons until they were injected into the QDs layer. As a result, the radiation recombination rate of the QDs layer was

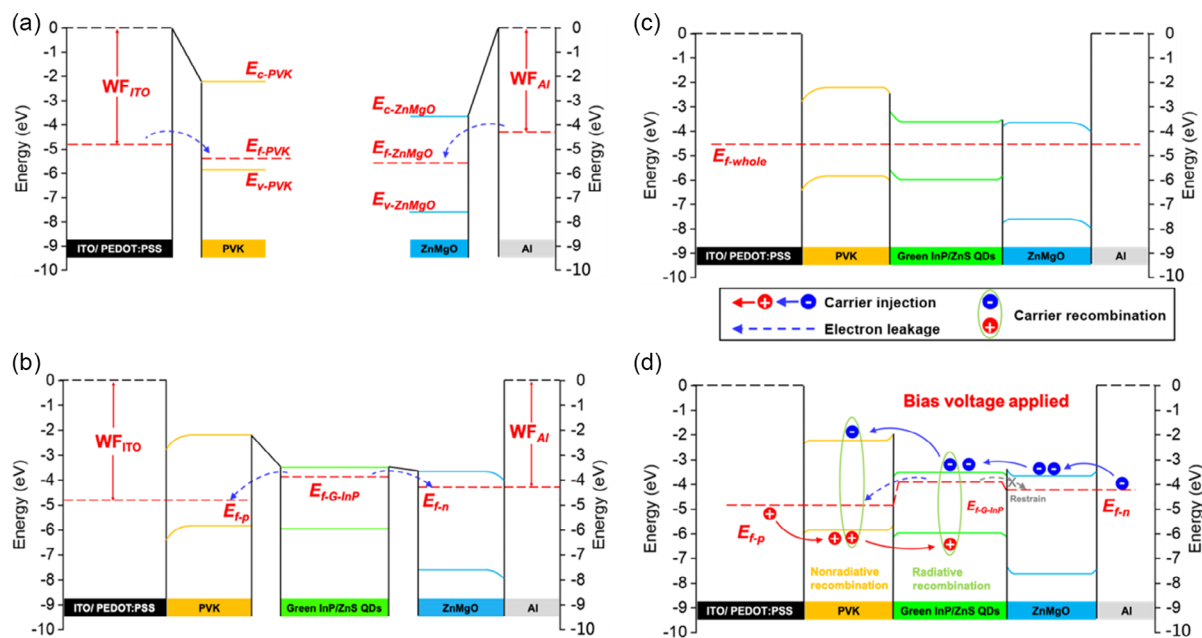


Figure 3. Schematics of energy bands in green InP QLED at different stages: a) before hole transport layer (HTL) and electron transport layer (ETL) contacted with electrodes, b) HTL and ETL contacted with electrodes while the QDs layer was independent, c) a complete green InP QLED with no bias voltage, and d) the dual effects of diffusion and migration driving excess electrons into the HTL.

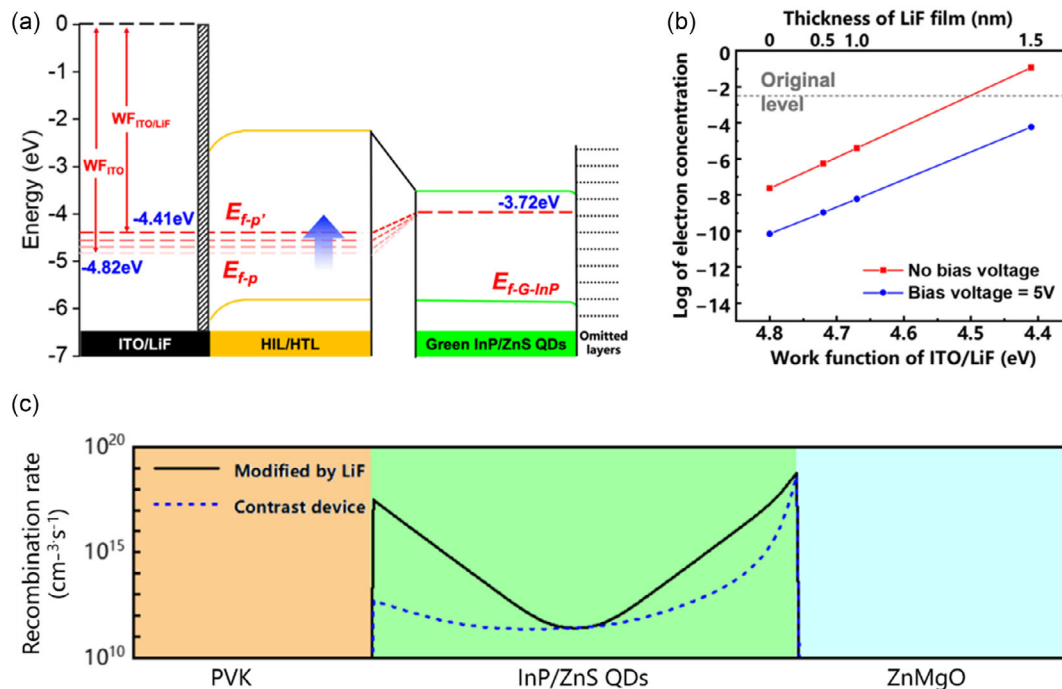


Figure 4. a) Schematics of the electron leakage trends in the green InP QLEDs with anodes at different work functions. b) Simulation of the electron concentration in the green InP QLEDs with anodes modified by different thickness LiF layers. c) Simulation of the radiation recombination rate in the green InP QLEDs.

significantly enhanced in the green InP QLEDs (Figure 4c), further confirming the existence of electronic leakage and the positive effect of the solution.

To further verify the effect of the LiF modification on the simulation results, we fabricated green InP QLEDs with green InP/ZnS QDs and characterized them to demonstrate the

confinement of electron leakage. The purchased green InP/ZnS QDs had an average size of 5.0 ± 0.2 nm and the ligands used were TOP and OA (Figure S5, Supporting Information). A typical device structure with a LiF layer is shown in Figure 5a, and a device without LiF modification was fabricated for comparison. Figure 5b shows the electroluminescence spectra of the proposed QLEDs. A negligible shift (<1 nm) was observed between these devices. The inset graph shows the pure and bright light-green emissions of the InP QLED device at a 5 V bias. Figure 5c shows the $J-V-L$ characteristics. With the addition of the LiF layer, the current density of the QLEDs decreased with an increase in resistance and increased owing to effective modification. The final results of the current density display also reflected the competitive results of the two changing trends. The green InP QLEDs with 0.5 or 1.0 nm LiF exhibited higher J values (240.30 and 229.90 mA cm $^{-2}$) than the contrast device (212.00 mA cm $^{-2}$) @5 V. The device with 1.5 nm LiF had a lower J (208.80 mA cm $^{-2}$ @5 V), which was an interesting phenomenon in contrast to the prediction. J may have had a lower value than that shown in the inset graph in the low-voltage region compared with the contrast device. Here, the increase in current density at higher voltages was caused by the strengthening of hole injection and hence is beneficial for achieving highly efficient QLEDs. This phenomenon is due to the tunneling effect, which is specifically analyzed later. In addition, the enhanced hole injection and confinement of leaked electrons promoted the recombination rate in the QDs layer. Consequently, the maximum luminance of the green InP QLED increased from 22 149 to 32 380 cd m $^{-2}$, an overall improvement of ≈ 1.46 times. This is shown in Figure 5d. The maximum EQE of our green InP QLEDs increased from

4.70% @ 5.92 mA cm $^{-2}$ (No LiF) to 9.14% @ 12.83 mA cm $^{-2}$ (LiF thickness = 1.0 nm, WF_{ITO} = 4.62 eV) which was an enhancement of approximately two times. Figure S6, Supporting Information, shows the EQE of more devices with different LiF layers (0, 0.5, 0.75, 1.0, 1.25, 1.5, 1.75, and 2.0 nm); LiF was credibly effective in improving the maximum EQE from 5.04% to 7.98% on average. The average maximum EQE was enhanced, which confirmed that good electron confinement and increased radiation recombination were achieved by the LiF modification.

Although enhanced hole injection achieved better performance in green InP QLEDs in this study, we are still curious about the abnormal decrease in current density in the low-voltage region. Figure 6a shows the $J-V$ of the HOD. The current density at low voltages (<2 V) of the HOD revealed the confinement of the carrier injection for the LiF-modified device. When the applied voltage was higher than 2 V, the ultrathin LiF layer exhibited an apparent effect on hole injection in the HOD. Similar phenomena have been reported and attributed to the tunneling effect (Figure 6b).^[33] In the original QLED devices, PEDOT:PSS contacted the ITO anode and its energy band was bent, as shown in Figure 6c. Therefore, holes must tunnel through the energy barrier. In the presence of an ultrathin LiF film of proper thickness, the voltage drop across the LiF film decreased the difference between the Fermi level of ITO and the HOMO of PEDOT:PSS (Figure 6d). This reduced the energy barrier through which the holes tunnel from the ITO to PEDOT:PSS, thereby increasing the injection current of the holes. Evidently, after LiF modification, the hole tunneling effect resulted in a better balance between electron and hole injection. This enhanced radiation recombination in the QDs layer, resulting in a high efficiency of the green InP QLEDs.

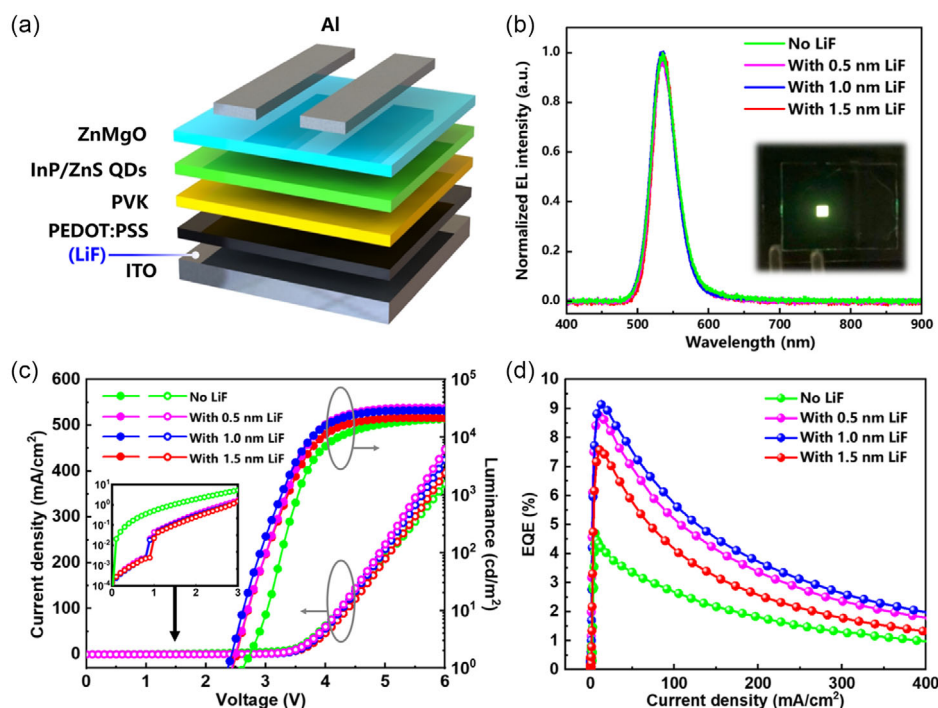


Figure 5. a) Device structure of typical green InP QLEDs with an ultrathin LiF layer. b) electroluminescence spectra at the same measuring condition (5 V). Inset: photograph of the operating device. c) Current density–voltage–luminance ($J-V-L$) characteristics. Inset: Current density–voltage ($J-V$) characteristics in log scale in the low-voltage region. d) External quantum efficiency (EQE)– J characteristics.

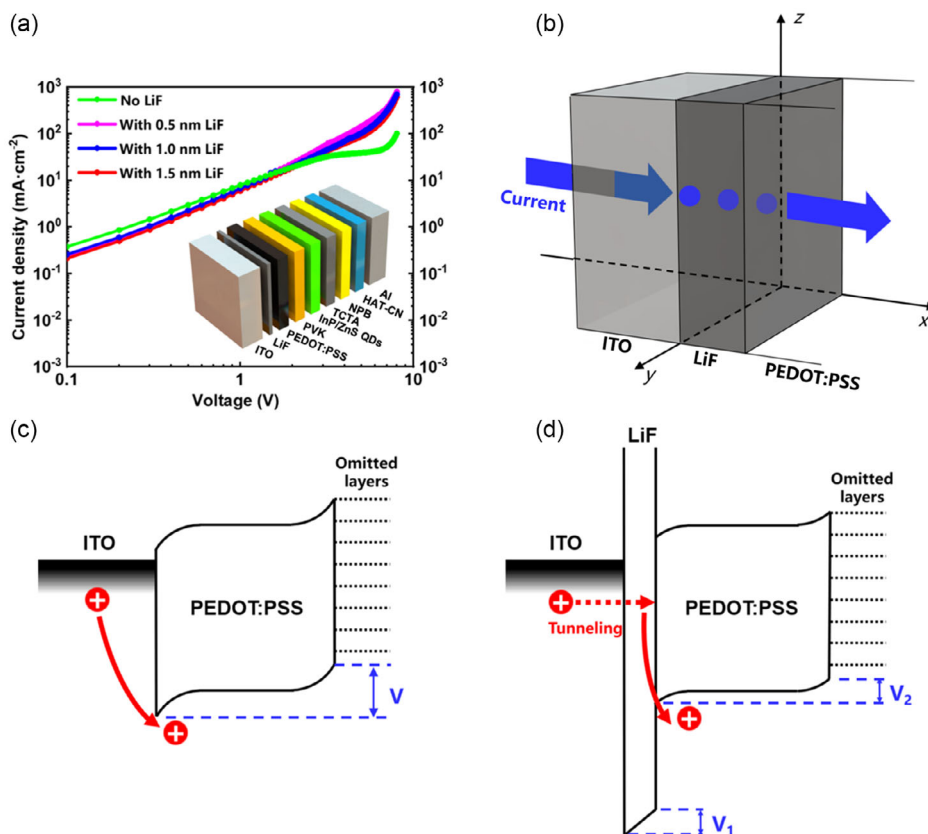


Figure 6. a) *J*–*V* profiles of the hole-only devices with modification using LiF of different thicknesses. b) Schematic of hole-tunneling injection from ITO into PEDOT:PSS through the surface between LiF and PEDOT:PSS layers. Schematic of energy diagram of the device c) without and d) with an ultrathin LiF layer.

4. Conclusion

This article reveals the electron leakage phenomenon in green InP QLED devices and a special mechanism by which it leads to carrier imbalance. In this study, the large Fermi energy difference between the green InP/ZnS QDs and ITO anode was considered to be the main driver of electron leakage. Using the designed experiments and simulations, we determined the path of the leaked electrons and confirmed the effect of the LiF modification. By applying ultrathin LiF layers of different thicknesses, WF_{ITO} could be adjusted from 4.82 to 4.41 eV (reaching the best modification effect at 4.62 eV). Consequently, electron leakage was hindered in the green InP QLEDs because of the reduced Fermi energy difference. In addition to the confinement of electron leakage, the ultrathin LiF layer also improved hole injection through the tunneling effect; hence, a more balanced carrier injection was achieved in the green InP QLEDs. Benefitting from hindered electron leakage and strengthened hole injection, a green InP QLED achieved an enhanced EQE of 9.14%, indicating a feasible approach for promoting green InP QLED performance.

Supporting Information

Supporting Information is available from the Wiley Online Library or from the author.

Acknowledgements

T.Q.Z. and F.Q.Z. contributed equally to this work. This work was supported by National Key Research and Development Program of China (grant no. 2022YFB3606504), National Natural Science Foundation of China (grant no. 62122034), Guangdong Basic and Applied Basic Research Foundation (grant no. 2022A1515011071), Shenzhen Basic Research General Program (grant nos. JCY20210324104413036 and JCY20190809152411655), Shenzhen Stable Support Research Foundation (grant no. 20220717215521001), and Natural Science Foundation of Top Talent of Shenzhen Technology University (SZTU) (grant no. GDRC202110). G. X. acknowledges the Science and Technology Development Fund, Macao SAR (file nos. FDCT-0044/2020/A1 and 0082/2021/A2), UM's research fund (file no. MYRG2020-00151-IAPME), the Natural Science Foundation of China (grant nos. 61935017 and 62175268), Guangdong-Hong Kong-Macao Joint Laboratory of Optoelectronic and Magnetic Functional Materials (grant no. 2019B121205002), and Shenzhen-Hong Kong-Macao Science and Technology Innovation Project (Category C) (grant no. SGDX2020110309360100).

Conflict of Interest

The authors declare no conflict of interest.

Data Availability Statement

The data that support the findings of this study are available from the corresponding author upon reasonable request.

Keywords

carrier injection balance, electron leakage, indium phosphide, quantum-dot light-emitting diodes (QLEDs)

Received: April 29, 2023

Revised: July 30, 2023

Published online: September 6, 2023

- [1] V. L. Colvin, M. C. Schlamp, A. P. Alivisatos, *Nature* **1994**, 370, 354.
- [2] X. L. Dai, Z. X. Zhang, Y. Z. Jin, Y. Niu, H. J. Cao, X. Y. Liang, L. W. Chen, J. P. Wang, X. G. Peng, *Nature* **2014**, 515, 96.
- [3] J. J. Hao, H. C. Liu, J. Miao, R. Lu, Z. M. Zhou, B. X. Zhao, B. Xie, J. J. Cheng, K. Wang, M. H. Delville, *Sci. Rep.* **2019**, 9, 12048.
- [4] W. R. Cao, C. Y. Xiang, Y. X. Yang, Q. Chen, L. W. Chen, X. L. Yan, L. Qian, *Nat. Commun.* **2018**, 9, 2608.
- [5] J. H. Jo, J. H. Kim, S. H. Lee, H. S. Jang, D. S. Jang, J. C. Lee, K. U. Park, Y. Choi, C. Ha, H. Yang, *J. Alloys Compd.* **2015**, 647, 6.
- [6] H. C. Liu, H. Y. Zhong, F. K. Zheng, Y. Xie, D. P. Li, D. Wu, Z. M. Zhou, X. W. Sun, K. Wang, *Chin. Phys. B* **2019**, 28, 128504.
- [7] J. Z. Song, J. H. Li, X. M. Li, L. M. Xu, Y. H. Dong, H. B. Zeng, *Adv. Mater.* **2015**, 27, 7162.
- [8] X. M. Li, Y. Wu, S. L. Zhang, B. Cai, Y. Gu, J. Z. Song, H. B. Zeng, *Adv. Funct. Mater.* **2016**, 26, 2435.
- [9] Z. C. Li, Z. M. Chen, Y. C. Yang, Q. F. Xue, H. L. Yip, Y. Cao, *Nat. Commun.* **2019**, 10, 1027.
- [10] P. Liu, Y. J. Lou, S. H. Ding, W. D. Zhang, Z. H. Wu, H. C. Yang, B. Xu, K. Wang, X. W. Sun, *Adv. Funct. Mater.* **2021**, 31, 2008453.
- [11] D. Battaglia, X. G. Peng, *Nano Lett.* **2002**, 2, 1027.
- [12] L. Li, P. Reiss, *J. Am. Chem. Soc.* **2008**, 130, 11588.
- [13] H. Moon, W. Lee, J. Kim, D. Lee, S. Cha, S. Shin, H. Chae, *Chem. Commun.* **2019**, 55, 13299.
- [14] S. H. Guo, Q. Q. Wu, L. Wang, F. Cao, Y. J. Dou, Y. M. Wang, Z. J. Sun, C. X. Zhang, X. Y. Yang, *IEEE Electron Device Lett.* **2021**, 42, 1806.
- [15] Q. Su, H. Zhang, S. M. Chen, *Appl. Phys. Lett.* **2020**, 117, 053502.
- [16] W. C. Chao, T. H. Chiang, Y. C. Liu, Z. X. Huang, C. C. Liao, C. H. Chu, C. H. Wang, H. W. Tseng, W. Y. Hung, P. T. Chou, *Commun. Mater.* **2021**, 2, 96.
- [17] X. Y. Yang, D. W. Zhao, K. S. Leck, S. T. Tan, Y. X. Tang, J. L. Zhao, H. V. Demir, X. W. Sun, *Adv. Mater.* **2012**, 24, 4180.
- [18] X. Y. Yang, Y. Divayana, D. W. Zhao, K. S. Leck, F. Lu, S. T. Tan, A. P. Abiyasa, Y. B. Zhao, H. V. Demir, X. W. Sun, *Appl. Phys. Lett.* **2012**, 101, 233110.
- [19] J. Lim, W. K. Bae, D. Lee, M. K. Nam, J. Jung, C. Lee, K. Char, S. Lee, *Chem. Mater.* **2011**, 23, 4459.
- [20] J. H. Jo, J. H. Kim, K. H. Lee, C. Y. Han, E. P. Jang, Y. R. Do, H. Yang, *Opt. Lett.* **2016**, 41, 3984.
- [21] I. Jang, J. Kim, C. Ippen, T. Greco, M. S. Oh, J. Lee, W. K. Kim, A. Wedel, C. J. Han, S. K. Park, *Jpn. J. Appl. Phys.* **2015**, 54, 02BC01.
- [22] H. C. Wang, H. Zhang, H. Y. Chen, H. C. Yeh, M. R. Tseng, R. J. Chung, S. Chen, R. S. Liu, *Small* **2017**, 13, 1603962.
- [23] Y. Deng, X. Lin, W. Fang, D. Di, L. Wang, R. H. Friend, X. Peng, Y. Jin, *Nat. Commun.* **2020**, 11, 2309.
- [24] Z. H. Wu, P. Liu, W. D. Zhang, K. Wang, X. W. Sun, *ACS Energy Lett.* **2020**, 5, 1095.
- [25] H. Zhang, N. Hu, Z. P. Zeng, Q. L. Lin, F. J. Zhang, A. W. Tang, Y. Jia, L. S. Li, H. B. Shen, F. Teng, Z. L. Du, *Adv. Opt. Mater.* **2019**, 7, 9.
- [26] F. Cao, S. Wang, F. J. Wang, Q. Q. Wu, D. W. Zhao, X. Y. Yang, *Chem. Mat.* **2018**, 30, 8002.
- [27] J. Kwak, W. K. Bae, D. Lee, I. Park, J. Lim, M. Park, H. Cho, H. Woo, D. Y. Yoon, K. Char, S. Lee, C. Lee, *Nano Lett.* **2012**, 12, 2362.
- [28] J. Ouyang, *Displays* **2013**, 34, 423.
- [29] Y. H. Kim, C. Sachse, M. L. Machala, C. May, L. Muller-Meskamp, K. Leo, *Adv. Funct. Mater.* **2011**, 21, 1076.
- [30] H. X. Luo, W. J. Zhang, M. L. Li, Y. X. Yang, M. X. Guo, S. W. Tsang, S. Chen, *ACS Nano* **2019**, 13, 8229.
- [31] H. Cho, D. Kang, Y. Lee, H. Bae, S. Hong, Y. Cho, K. Kim, Y. Yi, J. H. Park, S. Im, *Nano Lett.* **2021**, 21, 3503.
- [32] P.-C. Chiu, S.-H. Yang, *Nanoscale Adv.* **2020**, 2, 401.
- [33] Z. X. Wu, L. D. Wang, H. F. Wang, Y. D. Gao, Y. Qiu, *Phys. Rev. B* **2006**, 74, 165307.